Research Article

# P type copper doped tin oxide thin films and p-n homojunction diodes based on them

Ebitha Eqbal [a],[b], E.I. Anila [a],[c],*

[a] *Optoelectronic and Nanomaterials' Research Laboratory, Department of Physics, Union Christian College, Aluva, 683102, Kerala, India*
[b] *Department of Basic Sciences and Humanities, KMEA Engineering College, Aluva-683561, India*
[c] *Department of Physics and Electronics CHRIST (Deemed to be University), Bengaluru, 560029, India*

ABSTRACT

P-type copper doped tin oxide ($SnO_2$:Cu) thin films were prepared by chemical spray pyrolysis method on glass substrates for different doping concentrations. Their structural, optical, surface morphological, elemental and electrical studies were investigated. We fabricated two transparent homojunction diodes using optimized sample of $SnO_2$:Cu which are p-$SnO_2$:Cu/n-$SnO_2$ and p-$SnO_2$:Cu/n-$SnO_2$:F.These diodes are reported for the first time by this method.

## 1. Introduction

There is an extensive variety of transparent conducting oxides (TCOs) obtainable for wide applications in optoelectronic devices [1]. Distinctive commercially active TCOs are greatly n-type doped wide bandgap oxide materials such as indium tin oxide (ITO), doped zinc oxide (ZnO:Al, ZnO:Ga, ZnO:In), fluorine doped tin oxide (FTO) etc. Due to their commercial success, wide research is being undertaken to find viable hole conducting counterparts (p-type TCOs). There are several reasons for the deficiency of p-type TCOs. In order to achieve p-type conductivity, a material with a relatively low work function is required. The metal oxide systems such as tin oxide are characterized by relatively large work functions due to the nature of the metal – oxygen bond. The size differences in cation (anion) dopant with respect to those comprising the base material is another reason. The robust localization of O 2p states that form the upper edge of the valence band also cause trouble in producing p-type TCO's. Oxides showing p-type conductivity have been found in delafossite crystal structure family [2,3], corundum-type oxides [4] etc. Apart from discovering new p-type transparent conductors, there is a parallel effort to transform the usual n-type oxides such as ZnO and $SnO_2$ to p-type compounds in order to obtain p-type TCOs for application in the field of optoelectronic device technology.

Tin oxide ($SnO_2$) is a transparent semiconductor with a direct optical band gap of about 3.6–4 eV [5]. The undoped $SnO_2$ is an n-type semiconductor due to the presence of intrinsic defects like oxygen vacancies.

When it is doped with suitable elements (Al, Cu, Ga, Fe etc), carrier transformation takes place and get transformed to p type semiconductor. The ionic radii of $Cu^{2+}$ is 0.73 Å. This is close to that of $Sn^{4+}$ (0.69 Å). The $Sn^{4+}$ ions substituted with $Cu^{2+}$ acts as an acceptor energy level near the valence band thus increasing the p-conductivity. There are a few reports of copper doped tin oxide thin films synthesized by chemical spray pyrolysis method [6,7].

In the present work, p-type $SnO_2$:Cu thin films have been prepared by spray pyrolysis (SP) technique at substrate temperature 350 °C for different doping concentrations. We fabricated two homojunction diodes p-$SnO_2$:Cu/n-$SnO_2$ and p-$SnO_2$:Cu/n-$SnO_2$:F using optimized sample of copper doped $SnO_2$ by spray pyrolysis method. These homojunction diodes based on p-$SnO_2$:Cu are reported for the first time.

## 2. Experimental

The $SnO_2$:Cu and $SnO_2$:F thin films were spray deposited on ultrasonically cleaned glass substrates using dihydrate stannous chloride ($SnCl_2 \cdot 2H_2O$), copper nitrate ($Cu(NO)_2 \cdot 3H_2O$) and ammonium fluoride ($NH_4F$) as tin, copper and fluorine precursors. Required amount of $SnCl_2 \cdot 2H_2O$ to make 0.2 M solution was dissolved in 5 ml of concentrated hydrochloric acid and was heated at 90 °C for 10 min. This mixture was diluted by adding distilled water up to 25 ml which served as the starting solution. For copper doping, copper nitrate dissolved in doubly distilled water (25 ml) was added to the above solution, so that copper doping was in the range of 1 at.%,3 at.%, 5 at. %, 7 at.% and 10

---
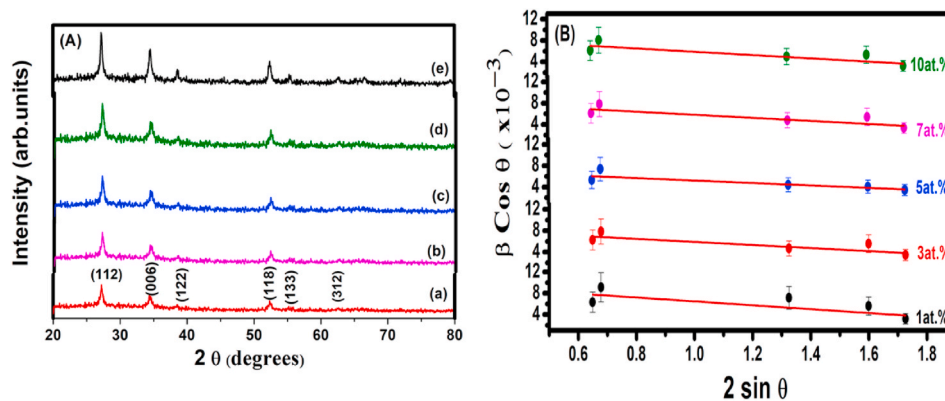
**Fig. 1.** (A) XRD spectrum of SnO$_2$:Cu thin film for (a) 1 at.% (b) 3 at.% (c) 5 at.% (d) 7 at.% (e) 10 at.% of Cu doping, (B) W–H plot of SnO$_2$:Cu thin films for different doping concentrations.

at.%. The spray solutions were magnetically stirred for 1 h before spraying on the substrate. Substrate temperature, spray rate, carrier gas pressure and source substrate distance were 350 °C, 10 ml/min, 0.2 kg/cm$^2$ and 15 cm respectively.

In the case of fluorine doping 50 ml aqueous solution of 10 at. % ammonium fluoride was added to 50 ml of 0.2 M starting solution. Substrate temperature was kept at 420 °C keeping all other spray parameters same as in the synthesis of SnO$_2$: Cu thin film.

The structural characterization of the SnO$_2$:Cu thin films were carried out using X-ray diffraction analysis (XRD) on a Bruker AXS D8 Advance diffractometer. Optical characterization of the SnO$_2$:Cu thin films were studied by using Shimadzu UV–Vis spectrophotometer model-UV 1800. The morphology and microstructure of the prepared films were studied by scanning electron microscopy (SEM) using JEOL JSM 6390LV. The elemental analysis was done using energy dispersive X-ray spectroscopy (EDX) using OXFORD XMX N. The thickness of the films were measured by ellipsometry using J.A.Woolam Co. Inc M 2000 ellipsometer. Ecopia HMS-5000 in Vander Pauw configuration was utilized for Hall effect measurements and I–V characteristics of diodes were studied using Keithley 2450 source measure unit.

## 3. Results and discussions

### 3.1. Structural analysis

To determine the crystal structure of the SnO$_2$:Cu thin films, X-ray diffraction techniques have been employed. The XRD spectra of SnO$_2$:Cu thin films is shown in Fig. 1(A). The grown films exhibit strong orientation along (112) plane and also other reflections are obtained from the planes (006), (122), (118), (224), (312) and (042) which are in agreement with the standard JCPDS file no:78–1063, having orthorhombic crystal structure. Thickness of SnO$_2$:Cu thin film samples gradually increases from 218 nm to 273 nm (Table 2) with increase in doping concentration. Intensity of XRD peaks also shows an increase with doping concentration indicating an improvement in crystallinity of samples.

There are two probable doping mechanism of SnO$_2$ with Cu (a) substitutional (b) interstitial. In the case of substitutional doping some Sn$^{4+}$ ions are replaced with Cu$^{2+}$ due to comparable ionic radii. The oxygen ion vacancies are created by substitutional doping of Sn$^{4+}$ whereas in the case of interstitial doping, Cu$^{2+}$ ions can occupy the interstitial site of SnO$_2$ lattice which can increase the tin ion vacancies for charge compensation [8].

The average grain size of sprayed SnO$_2$:Cu thin films for different doping concentrations was calculated using the Scherrer's formula [9].

$$D = \frac{0.9 \ \lambda}{\beta \ cos \ \theta} \tag{1}$$

Another relation used for the calculation of lattice strain and

**Table 1**
Grain size and lattice strain of SnO$_2$:Cu thin films.

| Doping concentration (at. %) | Grain size (D) from Scherrer's formula (nm) | Grain size (D) from W–H plot (nm) | Lattice Strain |
|---|---|---|---|
| 1 | 17.14 | 17.01 | −3.66 |
| 3 | 18.35 | 18.15 | −2.87 |
| 5 | 20.09 | 19.83 | −2.32 |
| 7 | 21.25 | 20.66 | −3.03 |
| 10 | 24.65 | 24.09 | −2.84 |

crystallite size [10] is,

$$\beta \ cos \ \theta = 0.9 \ \lambda/D + 2\xi sin\theta \tag{2}$$

where ξ represents the lattice strain and λ is the wavelength of X ray radiations, β is the full width at half maximum of the peak corresponding to the diffraction peak, θ is the glancing angle and D is the grain size of the thin film. From the slope and y intercept of the plot [WH plot] between 2sinθ and β*cos*θ [Fig. 1(B)], lattice strain and grain size were evaluated and they are tabulated in Table 1. It was observed that the grain size increases with Cu doping concentration. From the W–H plot for all the samples possess negative slope which is due to lattice compression behaviour.

### 3.2. Morphological and elemental analysis

Fig. 2 (a, b, c, d and e) depicts the FESEM images of the SnO$_2$:Cu thin films for different doping concentrations which reveals that the films have smooth surface with dense grains distributed throughout the surface. Particle size increases with doping concentration and at 10 at.% doping, the morphology changes to flower type. The EDX spectrum of the 5 at.% Cu doped sample is shown in Fig. 2(f). EDX analysis confirms the presence of Sn, O and Cu elements in the prepared SnO$_2$:Cu thin films.

### 3.3. Optical studies

The variation of transmission percentage with respect to wavelength of SnO$_2$:Cu thin films on quartz substrate for different copper doping levels is shown in Fig. 3(A). It was observed that the transmission percentage lies from 80 to 90% for wavelengths from 450 nm onwards in the visible region for the samples with Cu concentration 1, 3 and 5 at.%. For the other two samples (7 at.% and 10 at.% Cu) the transmission percentage lies in the range 65–80% in the same region. At higher doping concentrations, Cu atoms may occupy interstitial sites also and it causes a metallic nature to the thin films thereby decreasing the transmission percentage.

**Table 2**

Electrical studies of SnO$_2$:Cu thin films for different doping concentrations.

| Cu Doping Concentration (at.%) | Carrier Concentration (/cm$^3$) | Optical Band gap (eV) | Thickness (nm) | Resistivity (Ω.cm) | Conductivity (S/cm) | Mobility (cm$^2$/V.s) |
|---|---|---|---|---|---|---|
| 1 | $1.38 \times 10^{18}$ | 3.65 | 218 | 2.435 | 0.4107 | 1.86 |
| 3 | $3.07 \times 10^{18}$ | 3.72 | 224 | $3.8 \times 10^{-1}$ | 2.63 | 5.35 |
| 5 | $3.62 \times 10^{18}$ | 3.81 | 241 | $2.36 \times 10^{-1}$ | 4.22 | 7.28 |
| 7 | $8.63 \times 10^{18}$ | 3.36 | 258 | $1.75 \times 10^{-1}$ | 5.71 | 4.13 |
| 10 | $6.61 \times 10^{15}$ | 3.31 | 273 | $2.72 \times 10^{2}$ | 0.0365 | 34.6 |
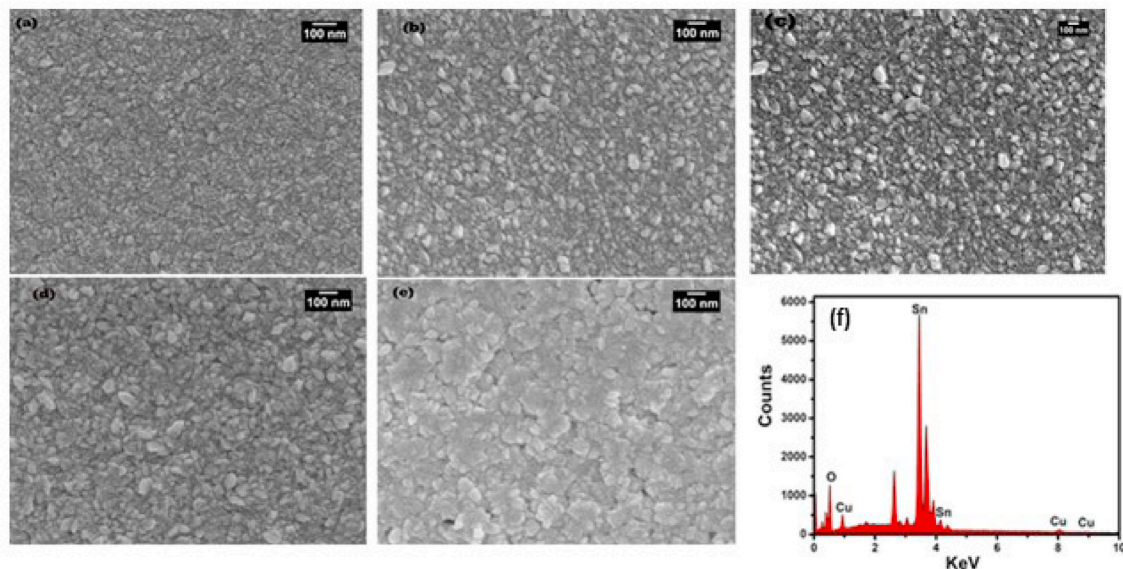


**Fig. 2.** SEM images of SnO$_2$:Cu thin films for different doping concentrations. (a) 1 at.%, (b) 3 at.%, (c) 5. at.%, (d) 7 at.% (e) 10 at.% and (f) EDX image of the sample synthesized at 5 at.% of Cu doping.
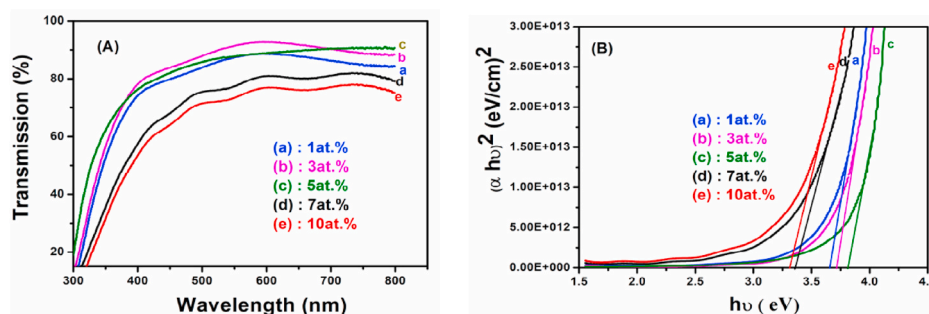


**Fig. 3.** (A) Transmission spectra and (B) Tauc plot of SnO$_2$:Cu thin films synthesized on quartz substrates.

The band gap determination was done by using the relation proposed by Tauc, Davis and Mott [11]. Fig. 3(B) shows the variation of $(\alpha h\upsilon)^2$ with h$\upsilon$ of SnO$_2$:Cu thin films. The optical band gap has then been determined by extrapolating the linear portion of the curve. The band gap was observed as varying in accordance with carrier concentration (Table 2) up to 5 at.% of doping concentration showing BM effect. For 7 at. % and 10 at. % of Cu doping, the band gap values are 3.36 eV and 3.31 eV which is less than that of bulk (3.6eV) and this may be attributed to band tailing effect. At higher doping concentrations, density of defect states increases drastically and it causes narrowing of band gap.

### 3.4. Electrical studies

The SnO$_2$:Cu thin films exhibited p-type conduction with mobility, hole concentration, and resistivity values as shown in Table 2. Depending on the density of defect states like tin interstitials, oxygen vacancies and copper at tin vacancy, the carrier concentration and conductivity level fluctuates.

It was observed that the conductivity of the film increased with Cu doping concentration up to 7 at.% and then decreased at 10 at.%. For the 10 at.% doped sample, the carrier concentration decreased drastically and because of that mobility increased to 34.6 cm$^2$/V.s. The decrease in conductivity of this sample may be because of the accumulation of Cu at grain boundary which may decrease the carrier concentration. The sample synthesized at 7 at.% of Cu doping shows maximum conductivity and carrier concentration. But mobility of this sample is less compared to the sample synthesized at 5 at.% doping. Hence SnO$_2$:Cu thin film synthesized at 5 at.% Cu doping was chosen for the fabrication of diode.
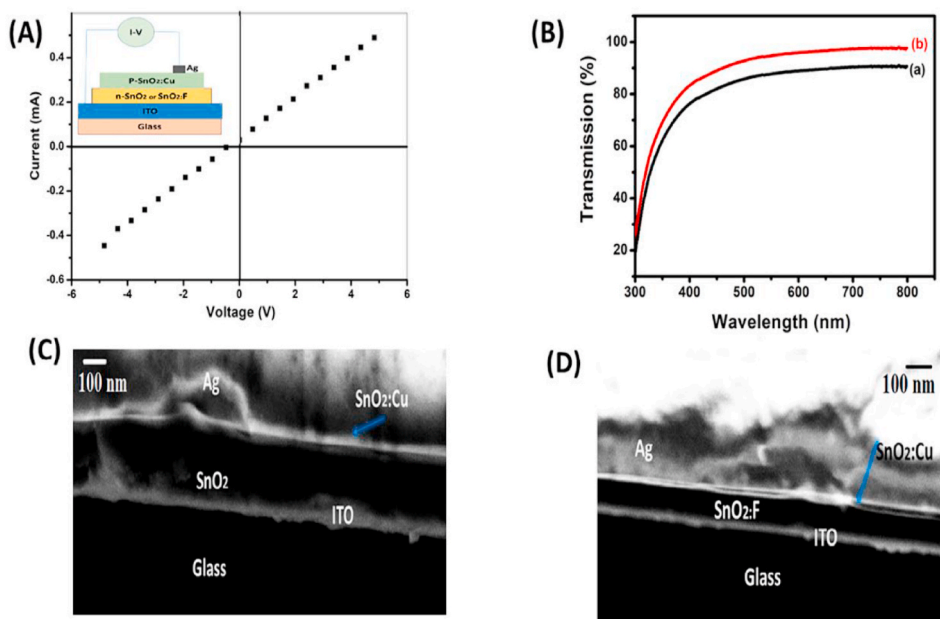
**Fig. 4.** (A) I–V Characteristics of SnO$_2$:Cu and Ag contact and inset shows schematic diagram of p-SnO$_2$:Cu/n-SnO$_2$(diode1) or p-SnO$_2$:Cu/n-SnO$_2$:F (diode2), (B) transmission spectra of (a) diode1 (b) diode2, (C) cross sectional FESEM of diode1and (D) diode2.

**Table 3**
Average thickness, carrier concentration and mobility of each layer of the diodes.

| Each layer of diode | Thickness (nm) | Carrier concentration (/cm$^3$) | Mobility (cm$^2$/V.s) |
|---|---|---|---|
| **n-SnO$_2$ (diode 1)** | 220 | $2.989 \times 10^{19}$ | 5.2 |
| **n-SnO$_2$:F (diode2)** | 302 | $8.67 \times 10^{20}$ | 4.61 |
| **p-SnO$_2$:Cu (diode 1 and diode2)** | 240 | $3.62 \times 10^{18}$ | 7.28 |

### 3.5. Fabrication of p-SnO$_2$:Cu/n-SnO$_2$ and p-SnO$_2$:Cu/n-SnO$_2$:F homojunction diodes

p-n junction diodes were fabricated using SnO$_2$:Cu (5 at.%) as p-layer and pure SnO$_2$ (diode1)/SnO$_2$:F (diode2) as n-layer on indium tin oxide (ITO) coated glass substrates (Inset of Fig. 4A). The spray parameters for both the layers were the same. 0.2 M solution of SnCl$_2$·2H$_2$O was used for the synthesis of n-SnO$_2$ layer of diode1 and 10 at.% of fluorine was used for doped n-SnO$_2$:F layer [12] of diode 2. Table 3 shows the thickness, carrier concentration and mobility of each layer of the diodes.

I–V characteristics of SnO$_2$:Cu and Ag contact is a straight line as shown in Fig. 4(A) which confirms the ohmic nature of contact. Fig. 4(B) shows transmission spectra of the diode 1 and diode2 respectively. We

can see that the average transmission percentage diode1 is 85% and for diode 2 is 90% in the visible region of electromagnetic spectrum. Fig. 4 (C and D) shows the cross sectional FESEM image of diode 1 and diode2 respectively, showing interface between various layers of the diode. Fig. 5(a and b) shows the I–V characteristics of diode 1 and diode 2 and they show rectifying behaviour.

Better rectification properties can be obtained by avoiding generation and recombination of carriers in the depletion region and inhomogeneity in barrier height. Parasitic series resistance and interface mismatch between the layers also affect the performance of diodes.

### 4. Conclusions

P-type copper doped thin films were prepared by chemical spray pyrolysis method on glass substrates for different doping concentrations. Among the synthesized samples, the sample synthesized at 5. at% of Cu doping shows better conductivity of 4.22 S/cm along with high mobility of 7.28 cm$^2$/V.s. Homojunction diodes, p-SnO$_2$:Cu/n-SnO$_2$ and p-SnO$_2$:Cu/n-SnO$_2$:F were fabricated for the first time by chemical spray pyrolysis. Both the diodes exhibited rectifying behaviour. We can improve diode characteristics by reducing interface problems between each layer.
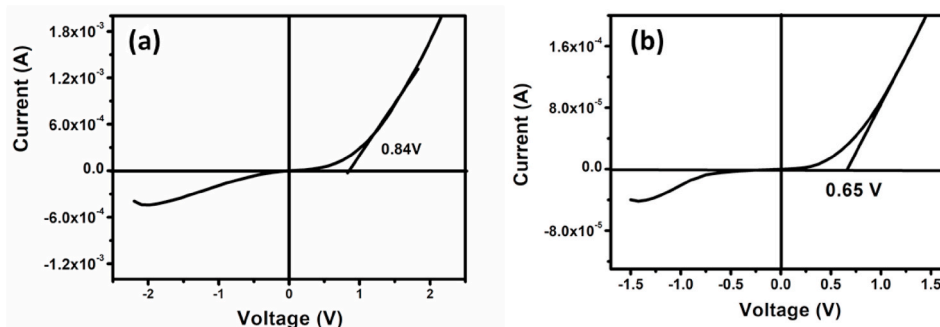


**Fig. 5.** I–V characteristics of (a) diode1 and (b) diode2.

## CRediT authorship contribution statement

**Ebitha Eqbal:** Conceptualization, Methodology, Investigation, Validation, Formal analysis, Writing – original draft. **E.I. Anila:** Project administration, Supervision, Writing – review & editing.

## Declaration of competing interest

The authors declare that they have no known competing financial interests or personal relationships that could have appeared to influence the work reported in this paper.

## References

[1] A. Stadler, Materials 5 (2012) 661.
[2] H. Kawazoe, M. Yasukawa, H. Hyodo, M. Kurita, H. Yanagi, H. Hosono, Nature 389 (1997) 939.
[3] M.K. Majee, P.A. Bhobe, U.P. Deshpande, A.K. Nigam, J. Appl. Phys. 122 (22) (2017) 225111.
[4] L. Farrell, K. Fleischer, D. Caffrey, D. Mullarkey, E. Norton, I.V. Shvets, Phys. Rev. B 91 (2015) 125202.
[5] M. Batzill, U. Diebold, Prog. Surf. Sci. 79 (2–4) (2005) 47.
[6] S.S. Roy, J. Podder, J. Optoelectron. Adv. Mater. 12 (7) (2010) 1479.
[7] G. Korotcenkov, I. Boris, B.K. Cho, Mater.Chem. Phys. 142 (1) (2013) 124.
[8] G.E. Patil, D.D. Kajale, D. D, S.D. Shinde, V.G. Wagh, V.B. Gaikwad, G.H. Jain, Advancement in Sensing Technology, Springer, Berlin, Heidelberg, 2013, p. 299.
[9] B.D. Cullity, S.R. Stock, Elements of X-Ray Diffraction, Prentice-Hall Inc., New York, 2001.
[10] G.K. Williamson, W.H. Hall, Acta Metall. Mater. 1 (1) (1953) 22.
[11] T.A. Safeera, N. Johns, E.I. Anila, A.I. Martinez, P.V. Sreenivasan, R. Reshmi, M. Sudhanshu, M.K. Jayaraj, J. Anal. Appl. Pyrol 115 (2015) 96.
[12] E. Eqbal, E.I. Anila, AIP Conf. Proc. 2082 (1) (2019), 030013.